Ainsalo, Ari; Sallinen, Reetu; Kaario, Ossi; Larmi, Martti

Optical investigation of spray characteristics for light fuel oil, kerosene, hexane, methanol and propane

Published in:
Atomization and Sprays

DOI:
10.1615/AtomizSpr.2019029626

Published: 01/01/2019

Document Version
Publisher's PDF, also known as Version of record

Please cite the original version:
Ainsalo, A., Sallinen, R., Kaario, O., & Larmi, M. (2019). Optical investigation of spray characteristics for light fuel oil, kerosene, hexane, methanol and propane. *Atomization and Sprays*, *29*(6), 521-544.
https://doi.org/10.1615/AtomizSpr.2019029626

OPTICAL INVESTIGATION OF SPRAY CHARACTERISTICS FOR LIGHT FUEL OIL, KEROSENE, HEXANE, METHANOL, AND PROPANE

Ari Ainsalo,[1*] Reetu Sallinen,[2] Ossi Kaario,[1] & Martti Larmi[1]

[1]Aalto University, Department of Mechanical Engineering, P.O. Box 14300, FIN-00076, Aalto, Finland

[2] Neste Corporation, P.O. Box 310, FIN-06101, Neste, Finland

Original Manuscript Submitted: xx/xx/xxxx Final Draft Received: xx/xx/xxxx

ABSTRACT

The present study investigates fuel spray penetration and opening angles for EN 590 light fuel oil, kerosene, hexane, methanol, and propane. Furthermore, droplet sizes are studied for methanol and light fuel oil sprays from a single location at the edge of the sprays. The fuels were injected from a marine-size common rail diesel injector to a spray chamber filled with nitrogen, and the results were based on the analysis of shadow images. The results indicated that propane sprays would penetrate slower and less than the sprays of the other fuels, but that the differences are decreased and finally almost disappeared when increasing chamber density. Apart from the lowest tested chamber density of 1.2 kg/m^3, propane formed significantly narrower sprays than the other fuels. With the exception of propane, the fuels had mostly similar responses to increased chamber densities. Variations between repetitions were large in relation to the differences in average values between the liquid fuels. Concerning droplet size measurements, the results suggested that methanol sprays would be characterized by slightly smaller droplet sizes than LFO sprays in the tested conditions. This finding is in line with an earlier study, albeit the found differences were smaller.

Keywords: Alternative fuel, kerosene, hexane, methanol, propane, image analysis, spray geometry, spray penetration, spray angle, droplet size

1 INTRODUCTION

Over the past decades, the awareness of harmful emissions related to internal combustion engines has increased considerably. Together with other aspects, such as resulting emission regulations, this has driven the research of alternative fuels that would be characterized by cleaner combustion and thus lower emissions. Due to their chemical compositions, methanol and propane enable clean combustion and low particulate emissions, which justifies their further research as motor fuels. Moreover, methanol can be seen as a potential biofuel (Dave 2008, Dolan 2010) that is capable of increasing the efficiency of spark-ignited engines (Brusstar et al. 2002, Nguyen et al. 2018). As this study focuses on diesel-type direct injection, light fuel oil (LFO) used in diesel engines will function as a primary reference fuel. Being used in aviation, kerosene is slightly lighter distillate than LFO and is included to the experiments in order to investigate the possible effects of slight changes in fuel properties. Hexane, on the other hand, has a known composition with five isomers and is a lighter distillate than kerosene but heavier than gaseous propane. As presented in the

subsequent chapter, all these fuels have different viscosities, densities, and surface tensions, which suggests that their sprays might have different characteristics. In this study, the fuels are injected from a high-pressure common rail diesel injector.

Macroscopic spray characteristics are typically described by tip penetration and opening angle. Particularly in compression-ignited engines, these parameters are of high importance as they have a significant effect on the mixing of fuel and air (Arai 2016, Heywood 1988, Hillamo 2011, Lefebvre 1989). In plain-orifice pressure atomizers, such as diesel injector nozzles, cone angle is largely dependent on the viscosity and surface tension of the liquid as well as the amount of turbulence in the jet (Lefebvre 1989). Several studies conducted with biodiesels indicate that fuels with higher viscosities, surface tensions, and densities have longer spray penetration and narrower opening angles (Deng et al. 2010, Desantes et al. 2009, Hwang et al. 2016, 2017, Li et al. 2006, Mohan et al. 2014), and the narrower sprays have also been found with biodiesel blends (Gupta and Agarwal 2016). The same effects of viscosity are also supported by Dernotte et al. (2012), albeit this study did not find a significant effect of surface tension. Furthermore, their results suggested that the effect of viscosity on opening angles would be decreased when increasing injection pressure. Besides the decreased effects of fuel properties, increased injection pressure has also been connected to reduced nozzle orifice geometry effects as concluded by Hulkkonen et al. (2015) who studied the effects of conical nozzle orifices on spray geometry.

Hulkkonen et al. (2011) have studied the differences between EN 590 diesel fuel and hydrotreated vegetable oil (HVO) in terms of spray geometry. Their results suggested that HVO, having little lower viscosity and density than the reference fossil diesel, would be characterized by slightly wider spray angles, whereas no significant difference was observed in penetration. Nevertheless, HVO sprays were reported to have higher spray tip velocities at the early stage of injection. With regard to the effects of increased ambient gas density/pressure, studies indicate both increased cone angles (Choi et al.2015, Desantes et al. 2006, Jun et al. 2001, Mohan et al. 2014, Sidu et al. 2001, Spiekermann et al. 2009) and slower penetration (Desantes et al. 2006, Naber and Siebers 1996). The slower penetration with increased chamber density is also observed in the experiments and simulations by Kaario et al. (2013) who studied chamber densities of 39 and 115 kg/m^3, the latter corresponding to peak cylinder pressures of approximately 300 bar.

In the analysis of sprays related to combustion or evaporation, Sauter mean diameter (SMD) is often used as a representative diameter (Arai 2016) as it describes the ratio of total liquid volume and total droplet surface area in a spray (Sirignano 1999), and because the rate of evaporation in droplets depends on surface area (Arai 2016). In the present study, droplet sizes are determined from shadow images, and this technique has been shown to be capable of having a good agreement with phase Doppler anemometry when studying moderately dense sprays with small diameters (Kashdan et al. 2004). Feasible consistency between shadowgraphy and other techniques has also been found by Berg et al. (2006), albeit they studied slightly larger particles. While Berg et al. (2006) conclude that all the tested methods are characterized by their own limitations and errors, they also suggest that shadow imaging would be the most suitable method for particle and velocity investigations in dense sprays. Besides these techniques, droplet sizes can also be analyzed by other techniques as presented by Coghe and Cossali (2012), Greenhalgh and Jermy (2002), Linne (2013), and Zhao (2012).

To the knowledge of the authors, very few publications exist concerning the characteristics of high-pressure kerosene, hexane, methanol, and propane sprays, which indicates a research gap and thus a need for new studies. In the present study, spray tip penetration and opening angles are determined for these fuels, and the results are compared with LFO sprays. Furthermore, due to the potential of methanol as a future biofuel, droplet sizes are investigated for methanol, LFO being again the reference fuel. In a study by Aigal et al. (1986), it was found that methanol sprays injected from a diesel injector would be characterized by smaller droplets than those of LFO, and this was taken, despite considerable differences in injection parameters, as a hypothesis for the performed experiments. In table 1, injection parameters and reported mean droplet size ranges for LFO have been collected from literature, which enables the evaluation of the performed LFO droplet sizing

results. Finally, regarding the spray opening angles, it is noted that angle definitions vary between publications (Dernotte et al. 2012, Desantes et al. 2009, Naber and Siebers 1996, Oguma et al. 2003, Shao et al. 2003, Wu et al. 2015, Yu et al. 2002), which should be considered when observing the results on spray geometry.

TABLE 1: Injection parameters and reported mean droplet size ranges for LFO/diesel in literature.

Parameter	Aigal et al. (1986) [1]	Cárdenas et al. (2010)	Dernotte et al. (2012) [2]	Hwang et al. (2017)	Kawaharada et al. (2015)	Komada et al. (2013)	Wu et al. (2015)
Nozzle orifice diameter [µm]	230	105 & 148	100	130	112	135	350
Injection pressure [MPa]	20...30 (peak)	60 & 110	30...150	40, 60, 80	65 & 135	80	22...31
Ambient pressure [MPa]	0.05 & 0.4	5	1	0.1	0.1	0.1	n/a
Ambient temperature [K]	n/a	800	297	300	296	≈ 296	n/a
Axial distance from injector [mm]	9...29	30 & 35	50	60...90	10 & 15	5, 7, 10, 15	80
Radial dist. from centerline [mm]	4...16	0...5	6...9 (edge)	0...3	0...1,5	0...2	n/a
Analysis method	Malvern	PDA	Malvern	PDI	L2F	L2F	Malvern
Mean size range, SMD [µm]	5.1...45.5	≈ 6...10	≈ 9...15	≈ 23,5...27	n/a	n/a	≈ 9…15
Mean size range, D10 [µm]	n/a	≈ 4...7	n/a	n/a	≈ 5...25	≈ 10...20	n/a

[1] For methanol, nozzle orifice diameter 320 µm and mean SMD size range 1.2...9.7 µm.

[2] The SMD range is for n-dodecane, density 749 kg/m^3, surface tension 25.3 mN/m, kinematic viscosity ≈ 1.9 mm^2/s.

2 METHODS

2.1 Experimented fuels

Table 2 presents densities, kinematic viscosities, and surface tensions for the tested fuels. Apart from propane, they are liquids at room temperatures and atmospheric pressures. While the properties found from literature may not be identical to the exact specifications of the tested fuels, the presented values indicate a clear order between the fuels in terms of the presented characteristics. The tested light fuel oil fulfilled European EN 590 requirements for automotive diesel fuels. While the standard allows variations in density and viscosity, the supplier of the LFO offered typical values of 840 kg/m^3 and 3.2 mm^2/s (at 313 K), respectively. The studied hexane was a mixture of hexane isomers, and the methanol was of laboratory grade with a minimum purity of 99.8%. Propane was stored in a commercial forklift LPG (liquid petroleum gas) bottle and had a purity of over 95% according to the supplier.

TABLE 2: Properties of experimented fuels from literature. The surface tensions of LFO not specifically for EN 590 fuels.

Fuel	Density [kg/m³] [1]	Kinematic viscosity at 293 K [mm²/s]	Surface tension at 293 K [mN/m]
LFO (EN 590)	820 – 845	2 – 4.5 (313 K) [1]	28 – 29.5 [4,5,6]
Kerosene	770 – 830	2 [3]	26 [7]
Hexane	660 [2]	0.5 [3]	18.4 [7]
Methanol	790	0.75 [1]	22.5 – 23 [8,9]
Propane (liq.)	510	0.19 [3]	6.4 (300 K) [7]

[1] Dietsche & Reif (2011), [2] Producer datasheet: 672 kg/m³, [3] Based on dynamic viscosity from Lefebvre (1989), [4] Wang et al. (2006), [5] Das et al. (2018), [6] Esteban et al. (2012), [7] Lefebvre (1989), [8] Jasper (1972), [9] Vázquez et al. (1995)

2.2 Test facilities

The experiments were conducted in a spray chamber designed for fuel spray measurements. The chamber, being filled with pressurized nitrogen, was equipped with two circular windows that provided an optical access to the sprays from opposite sides and thus enabled the use of backlight imaging method. The effective diameter of the borosilicate windows was 100 mm, and their

thickness was 55 mm to allow pressures up to 100 bar. The temperature of the chamber was not controlled, and it remained at approximately 290...300 K during the measurements. Table 3 presents the summary of test conditions, imaging parameters, and analysis techniques. Further explanations on the analysis methods shall be given in the following chapter.

TABLE 3: Summary of test conditions, imaging parameters, and analysis techniques.

		Measurement type	
		Spray geometry	Droplet sizes
Test environment	Test facility	Spray chamber, optical access from opposite sides	
	Chamber atmosphere	Pressurized nitrogen	
	Temperature	Room temperature, approx. 294 K	
	Chamber densities [kg/m^3]	1.2, 35 & 100	35 & 100
Fuels & injection	Injector body	Solenoid-driven, marine-size common rail diesel injector	
	Injector nozzle	8/9 orifices plugged, orifice diameter 0.3 mm, umbrella angle 153°	
	Injection pressures [Mpa]	55 & 100	
	Injection signal duration	2 ms	
	Fuels	LFO [1], Kerosene, Hexane, MeOH [2], Propane	LFO [1] & MeOH [2]
	MeOH lubrication additive	-	Ethomeen O/12, ≈ 1 m-%
Imaging	Imaging mode	High-speed (10 000 fps)	Single-shot
	Optics	50 mm, F/1.4	Long-distance microscope
	Image resolution	512x304 [3]	2048x2048
	Image area [mm^2]	79*47 or 81*48 [3]	2.64*2.64
	Backlight method	125 W DC halogen lamp	200 mJ Pulse laser
	Exposure time	≈ 3.3 µs [3]	≈ 20 ns
Image analysis	Analysis based on	Shadow images	
	Analysis software	In-house Matlab scripts	Commercial (Davis X by LaVision)
	Attributes to be analyzed	Penetration, opening angles	Mean droplet sizes & distributions

[1] EN 590 light fuel oil, [2] Methanol purity > 99.8 %, [3] For propane: resolution 512x256, image area 53*27 mm^2, and exposure time ≈ 8.3 µs.

Figure 1 illustrates the schematics of fuel and nitrogen systems for the employed test setup. The pressure inside the chamber was controlled by adjusting the pressure regulator, needle valve, and pressure control valve manually. Chamber density was determined from the readings of pressure and temperature sensors. With the lowest chamber density of 1.2 kg/m³, the pressure control valve was fully open, and the pressure inside the chamber was equal to the atmospheric pressure plus minor pressure losses in the exit pipe. During the acquisition of images for spray geometry analysis, a constant nitrogen flow was applied through the chamber. When taking images for droplet sizing, the chamber was filled with new nitrogen after every 10 injections.

The fuel pressure in the common rail was manually controlled by regulating the air pressure of the air-driven high-pressure (HP) fuel pump and adjusting the flow rate in the fuel return line. The fuel cooler shown in figure 1 was in use only when acquiring methanol spray images for geometry analysis. This prevented the exceedance of methanol's boiling point and thus its' abundant vaporization into the laboratory room. Based on experiments with LFO, it was concluded that the fuel cooler had no significant effect on spray geometry.

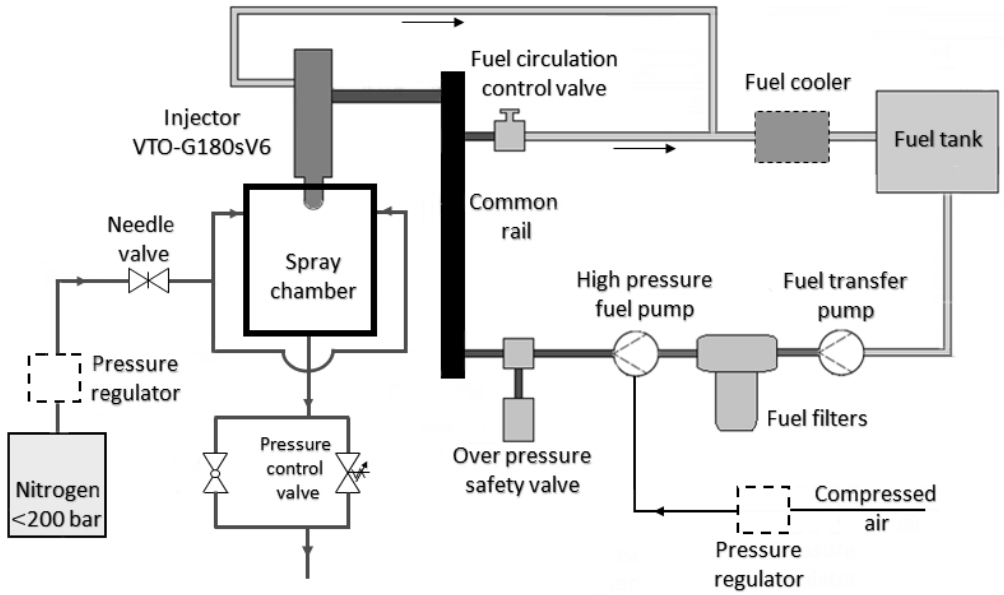

FIG. 1: Schematic flow chart for the fuel (excl. propane) and nitrogen systems of the experimental setup.

Due to its' low boiling point, propane required a special fuel system setup in order to keep the fuel in a liquid form. Instead of the fuel transfer pump and fuel filters shown in figure 1, a cooling system was built between the propane gas bottle and the HP fuel pump. This system comprised a freezer filled with ice as well as a fuel line coil inside the freezer to ensure efficient cooling. Moreover, a non-return valve was installed between the freezer and the HP fuel pump to prevent fuel backflow. Gaseous low-pressure propane from fuel return lines was directed away from the fuel system.

Figures 2 and 3 present schematic imaging system arrangements for the acquisition of spray geometry and droplet sizing images, respectively. Detailed information on imaging parameters has been listed in table 3. In order to achieve a flicker-free illumination, a direct current halogen lamp was used as a backlight in spray imaging. While the laser employed in droplet imaging had a typical pulse duration of 3...5 ns, the wavelength conversion into a non-coherent light prolonged the duration to approximately 20 ns. Furthermore, the droplet imaging system included an automatic background image subtraction.

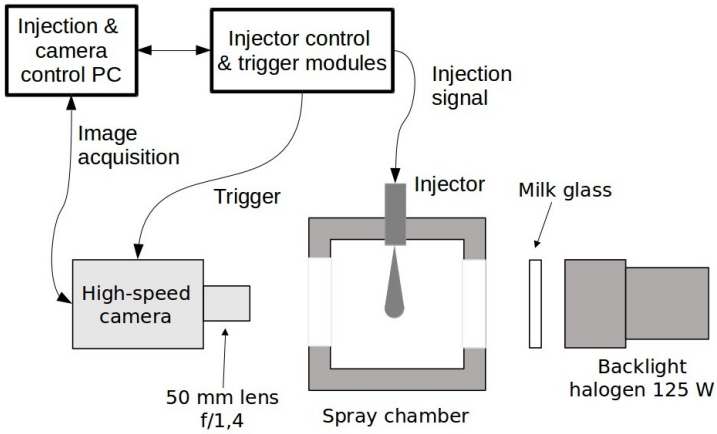

FIG. 2: Schematic representation of the imaging system arrangement for spray geometry measurements.

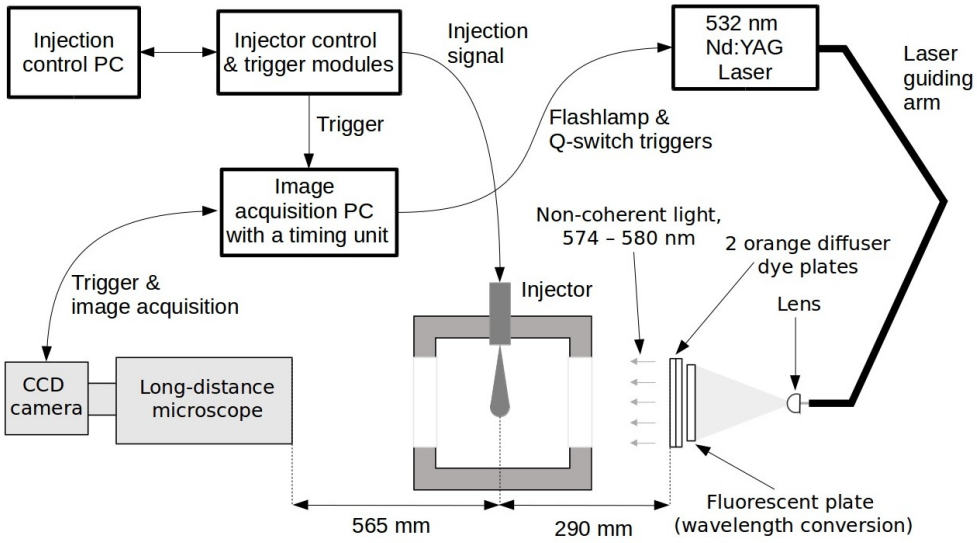

FIG. 3: Schematic representation of the imaging system arrangement for droplet size measurements.

2.3 Analysis methods

The analysis of spray geometry was conducted with in-house Matlab scripts that recognized the spray from the background on the basis of different intensity levels. The process of determining the spray area included intensity inversion, background subtraction, and intensity thresholding. Spray penetration was defined from the pixel within the spray area that had the longest distance from the nozzle orifice. The determination of an opening angle (θ in fig. 4) was based on finding the pixel that belongs to the spray area and has the longest perpendicular distance from the centerline of the spray (y) calculated at a given distance from the nozzle orifice (x). In other words, the script calculated the width of the half-spray at given distances from the injector nozzle. For the results presented in this paper, these distances were 20 mm and 40 mm. This procedure was applied for both spray edges, and the average of these two angles was considered in further data processing. All the results concerning spray penetration and opening angles were averaged over 50 (LFO and methanol) or 60 (kerosene, hexane, propane) consecutive injections, and the error bars shown in the results are based on standard deviation.

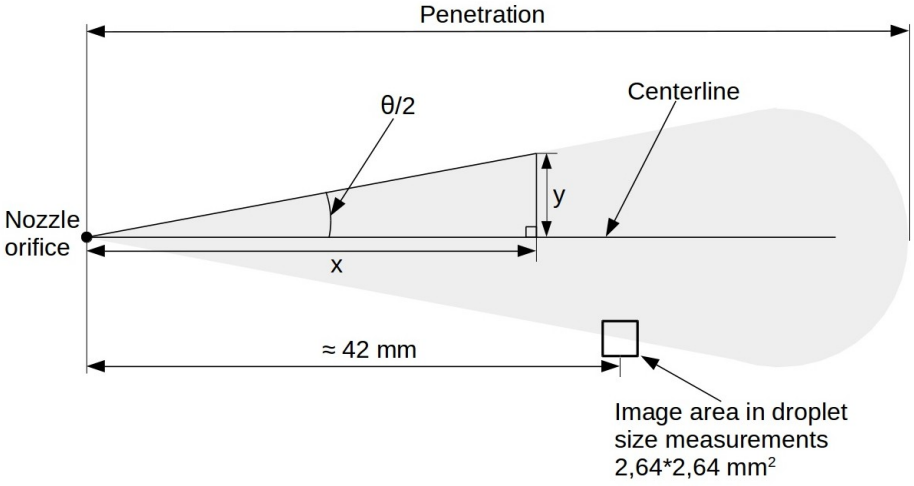

FIG. 4: Schematic representation on the determination of penetration and opening angle as well as the field of view in droplet images. X = 20 mm and 40 mm, y depends on the local width of the spray.

The determination of characteristic opening angles depended on the shape of the opening angle time histories. If a visible local minimum in the opening angle was observed before the end of injection (fig. 5, left), the characteristic opening angle was determined as the lowest value between initial and post-injection transients. If no local minimum existed before the end of injection (fig. 5, right), or if the time history was monotonically increasing until the end of injection, the characteristic angle was defined at the point of end of injection. The standard deviations for these angles were defined at the same points in time as the angles themselves. The methods for defining the opening/cone angles vary between publications (Dernotte et al. 2012, Desantes et al. 2009, Naber and Siebers 1996, Oguma et al. 2003, Shao et al. 2003, Wu et al. 2015, Yu et al. 2002), whereupon the results of this study concerning opening angles may not be quantitatively comparable with other studies. Finally, it was identified that the injection duration of 2 ms may have been too short for the spray to develop a steady-state opening angle value at longer distances from the nozzle.

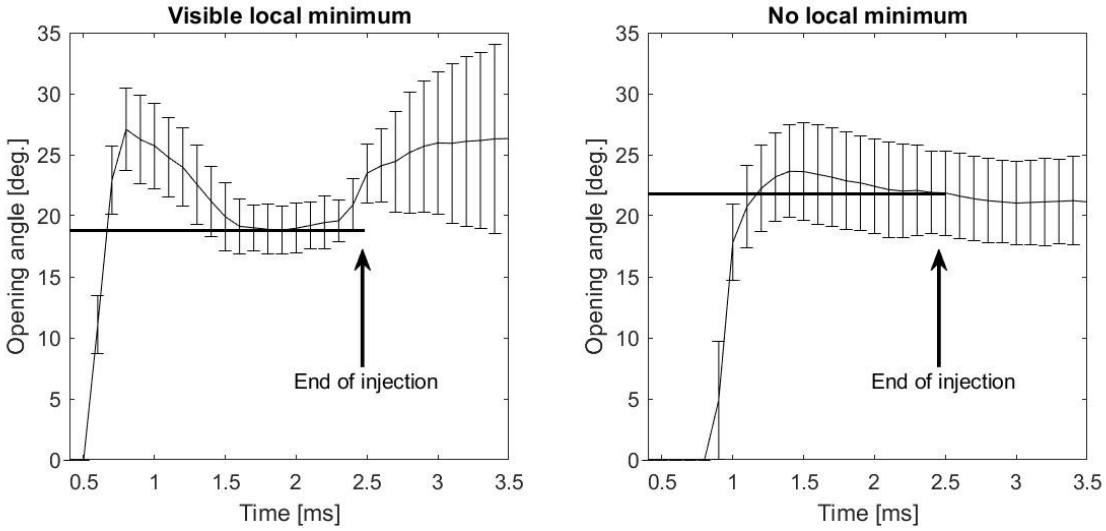

FIG. 5: Determination of characteristic opening angles from different time history shapes. Standard deviations also visible.

A proprietary analysis software (Davis 10 by LaVision GmbH) was employed for the detection of droplets from shadow images. The detected droplet areas with possibly arbitrary shapes were replaced by ellipses that fitted to the droplet shape (fig. 6). The centricity of a droplet was determined as the ratio between the short and long axes of the ellipse, and the droplet diameter was defined such that a circle with the specific diameter had the same area as the detected shadow area. The statistical weight of each detected droplet depended on diameter in order to consider the different detection probabilities between large and small droplets.

Table 4 presents the applied droplet analysis parameters, including minimum and maximum filters. The parameters were chosen after experimenting with several combinations in order to find a suitable compromise for the analyzed images. Minimum and maximum filters were included to further reduce the number of false detections. For instance, detected “droplets” with strong non-centricity were clearly false detections when observing detection results visually. An example on the effects of centricity parameter has been documented by Kashdan et al. (2004). The location of the field of view in droplet imaging with respect to the injector is shown in figure 4, albeit minor adjustments were necessary to capture the spray edge. As droplet velocities are generally lower far from the injector nozzle, the field of view was located rather far from the injector nozzle. The scaling of the images was conducted by placing a piece of millimeter paper into the focal point of the microscope and determining the pixel-to-micrometer ratio from the taken images.

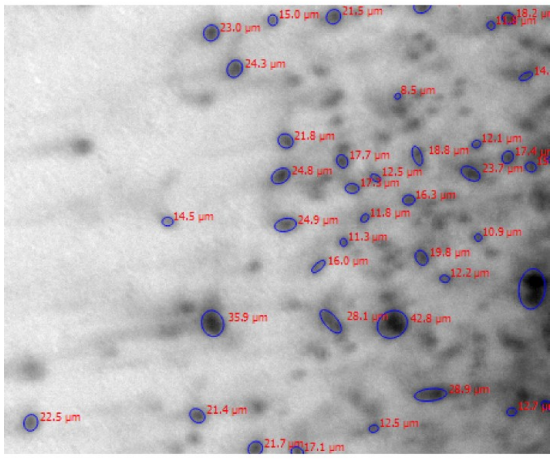

FIG. 6: Example of detected droplets.

TABLE 4: Droplet detection parameters

Parameter	Unit	Value
Normalization radius	px	4
Pixel noise reduction	-	Strong
Binarization threshold	%	35
Min. shadow area	px	7
Minimum slope	%	9
Minimum diameter	µm	5
Maximum diameter	µm	60
Minimum centricity	%	60

2.4 Uncertainties

The accuracy of image analysis is largely related to the calibration of pixel-to-length scale, motion blur, limited image resolution, and intensity thresholding. Furthermore, statistical error originates from spray-to-spray variations. Scale error was estimated to be around 1%, whereas the error of motion blur and resolution depended on measurement type. For spray geometry analysis, these were estimated to be around 0.7 mm (based on 3.3 µs exposure time and 200 m/s spray tip velocity) and approximately 0.3 mm (2 px when analyzing opening angles), respectively. Nevertheless, the error due to motion blur was lower for the determination of opening angles as the transversal velocities of sprays are much lower. It is also noted that while Kawaharada et al. (2015) and Komada et al. (2013) have measured even higher velocities than the 200 m/s close to the nozzle, spray tip velocities decrease rapidly when increasing the distance from the injector. Using a characteristic length of 20 mm, the errors of 0.7 mm and 0.3 mm correspond to relative errors of 3.5% and 1.5%, respectively. For propane image series, the motion blur error was larger due to the longer exposure time (table 3).

Assuming a speed of 50 m/s at the spray edge (location in fig. 4) and an exposure time of 20 ns, the motion blur for droplet sizing images was calculated to be 1 µm. With a characteristic length of 10 µm, the theoretical relative error due to motion blur becomes 10%. In practice, the error is lower due to intensity thresholding that excludes a part of the blurred tail. Moreover, smaller particles are known to have lower velocities, which further reduces the relative error. A theoretical resolution error of 2 pixels corresponds to approximately 2.6 um, which is considerable for the smallest detected droplets. Despite the magnitudes of these error sources, it was thought that more error originated from the limited image quality and hence the success of droplet detection. Optically challenging imaging environment was attributed to shallow depth of field, dense sprays, small droplets with high velocities, and the chamber windows that unavoidably induced some light

reflections and refraction. The analysis parameters were determined to work moderately well for all the image series, which inevitably resulted in varying detection success between individual images or droplets (fig. 6). The error arising from analysis has been identified by Kashdan et al. (2003, 2004) who found that the accuracy of image analysis is sensitive to thresholding, and that the sizes of small objects are underestimated, albeit post-processing was shown to facilitate the latter issue. Finally, it is noted that droplet sizes may vary significantly within a spray, which should be kept in mind when interpreting the results as this study investigated the droplet sizes in a single location at the edge of the sprays.

During the experiments, small variations around the target value had to be accepted in fuel pressures and chamber densities. The fluctuations in the moving average of fuel rail pressure were typically in the range of ± 2%, the worst cases being in the range of ± 5%. At the lowest chamber density of 1.2 kg/m^3, the chamber pressure could not be controlled because of the dependence on the atmospheric pressure. In practice, the measured values were slightly over 1.2 kg/m^3. At the elevated chamber densities of 35 and 100 kg/m^3, the accepted values typically deviated less than 2% or 1% from the target value, respectively.

3. RESULTS AND DISCUSSION

3.1. Visual observations

Figure 7 shows example spray images for all the fuels and chamber densities. The images have been taken at the same time with respect to injection signal, which allows to see the effect of chamber density and fuel on the shape and evolution of the spray. The differences between LFO, kerosene, hexane, and methanol sprays are rather small, particularly when taking the existence of spray-to-spray variations into consideration. However, propane differs from the other fuels. At the lowest chamber density of 1.2 kg/m³, propane seems to be characterized by a wider spray close to the injector nozzle. At elevated chamber densities, and especially at the density of 100 kg/m³, the fast evaporation of propane becomes obvious and results in shorter penetration and narrower spray angles. It is noted though that had the methods been able to reliably detect fuel vapor, the observations concerning propane spray geometry would have been different.

Despite losing information on the structures of spray edges, the averaging of images enables to visualize the differences in overall spray geometry. Figure 8 compares the evolution and shape of methanol and LFO sprays and includes all the tested chamber densities. In the images, each frame is an average of 50 shots. At the two higher densities, the differences between the fuels are small yet visible when carefully observing the shapes of the sprays. At the chamber density of 1.2 kg/m³, the differences become more obvious as the spray tips have notably different shapes.

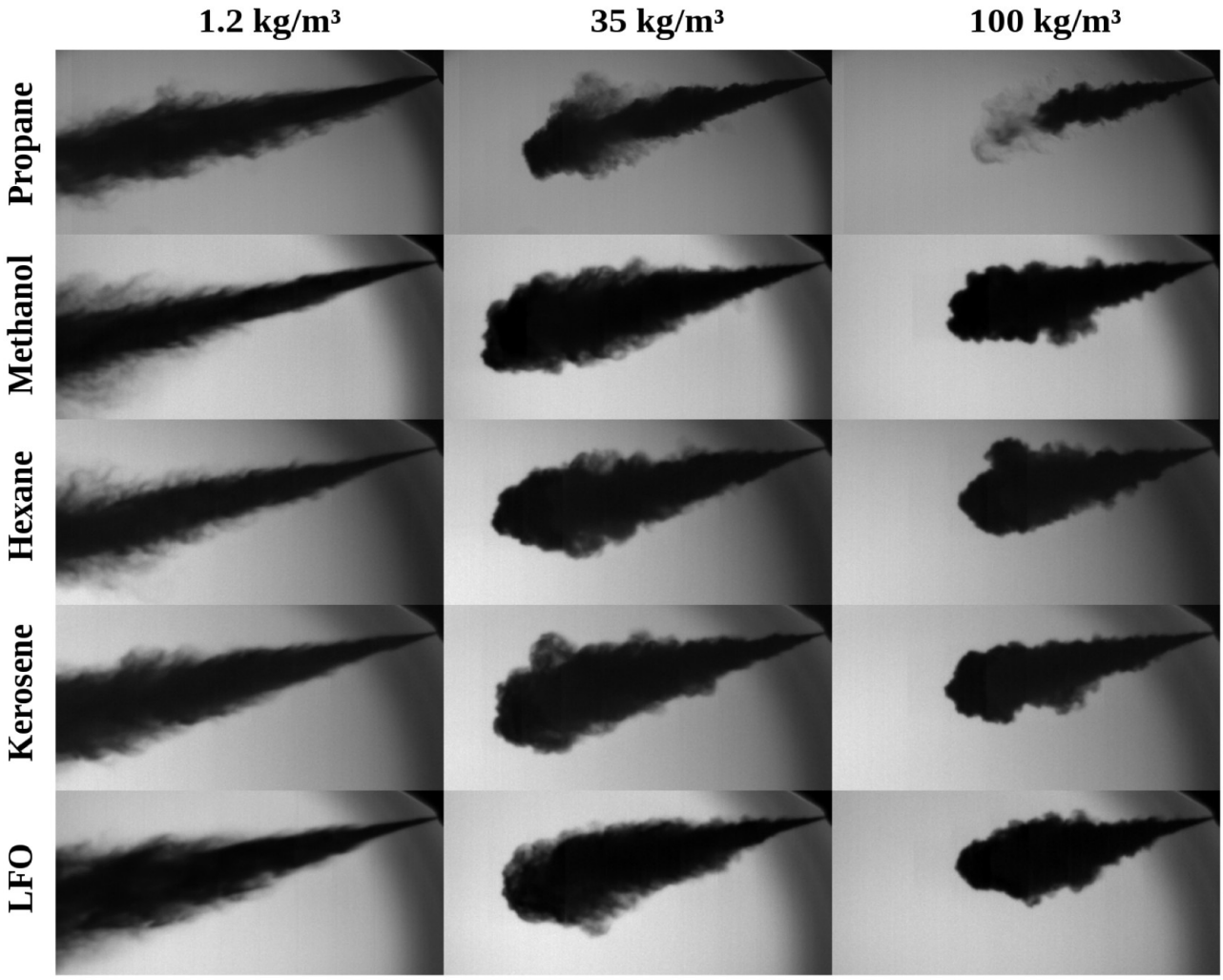

FIG. 7: Examples of fuel spray images taken at the same time with respect to injection signal. Injection pressure 1000 bar, image area 50*25 mm².

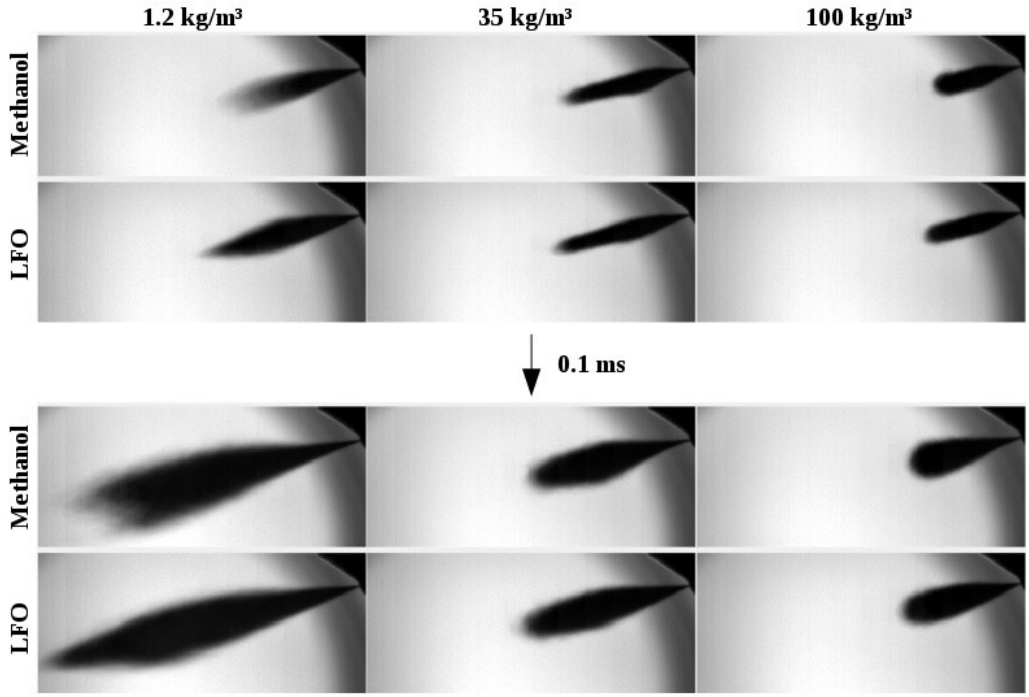

FIG. 8: Evolution and shape of average methanol and LFO sprays at different chamber densities. Start of injection approx. 0.1...0.15 ms before the upper image series. Images averaged over 50 shots. Injection pressure 1000 bar, image area 59*25 mm².

3.2 Penetration

Figures 9, 10, and 11 present spray tip penetrations for the chamber densities of 1.2, 35, and 100 kg/m³, respectively, and include both 550 and 1000 bar injection pressures. At the lowest chamber density, the differences between the liquid fuels are rather small especially with the higher injection pressure, whereas propane behaves differently. The error bars, showing the standard deviation of the repetitions, also indicate that the penetration length of propane sprays varies significantly between injections. This was thought to be the result of fast and varying vaporization rates. Due to the low chamber density, the spray tips accelerate fast and reach the limits of the image area within a narrow time window (fig. 9). When increasing chamber density, both standard deviations and the differences between propane and the liquid fuels seem to decrease. Furthermore, the acceleration and deceleration regions discussed by Hillamo (2011) can be identified from figures 10 and 11.

Overall, the differences between the liquid fuels are rather small also when increasing chamber density. However, with the combination of 550 bar injection pressure and 35 kg/m³ chamber density, fig. 10 indicates that LFO and methanol sprays would momentarily be characterized by longer penetrations. As this observation is inconsistent with the other shown test points, care should be taken not to give too much weight on these differences. Besides the aforementioned findings, figures 10 and 11 also suggest that the tip of LFO sprays would accelerate slightly more than the other fuels in the beginning, but that it would also decelerate faster after penetrating the first 30...35 mm. Finally, it is observed that an increased injection pressure decreases injection delay, which is in line with the findings of Hwang et al. (2017). In the figures, time is calculated from the start of injector energizing.

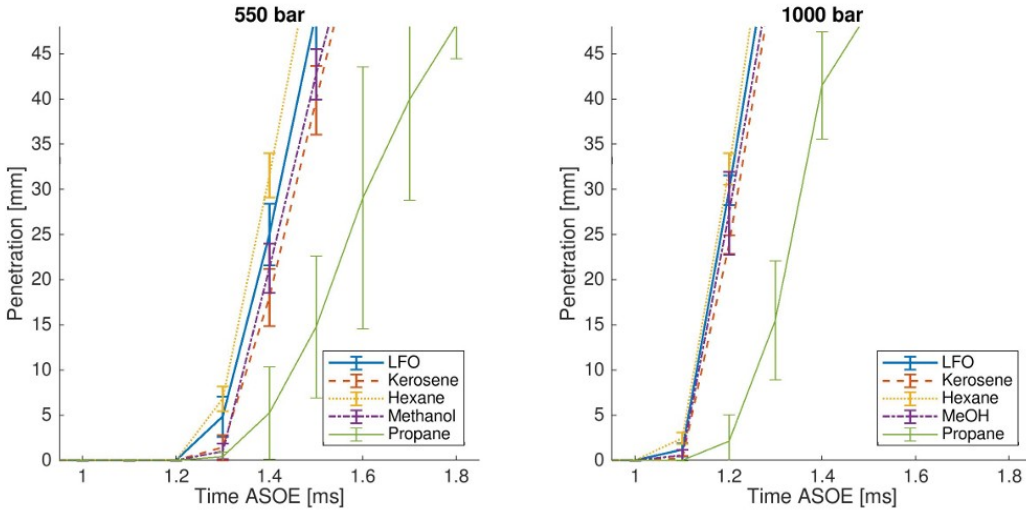

FIG. 9: Measured spray tip penetrations for the examined fuels. Chamber density 1.2 kg/m³, injection pressures 550 and 1000 bar. Error bars indicate standard deviation. ASOE: After start of energizing.

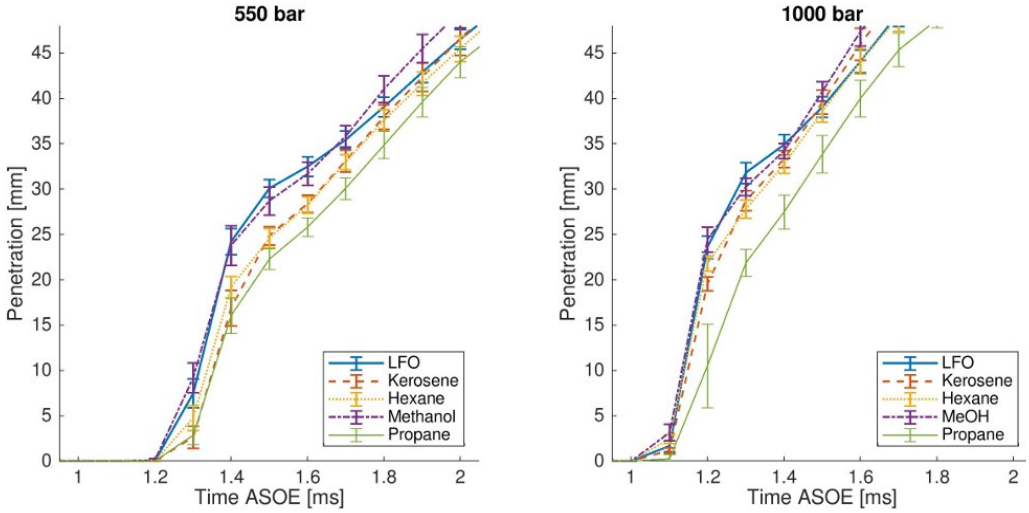

FIG. 10: Spray tip penetration, chamber density 35 kg/m³.

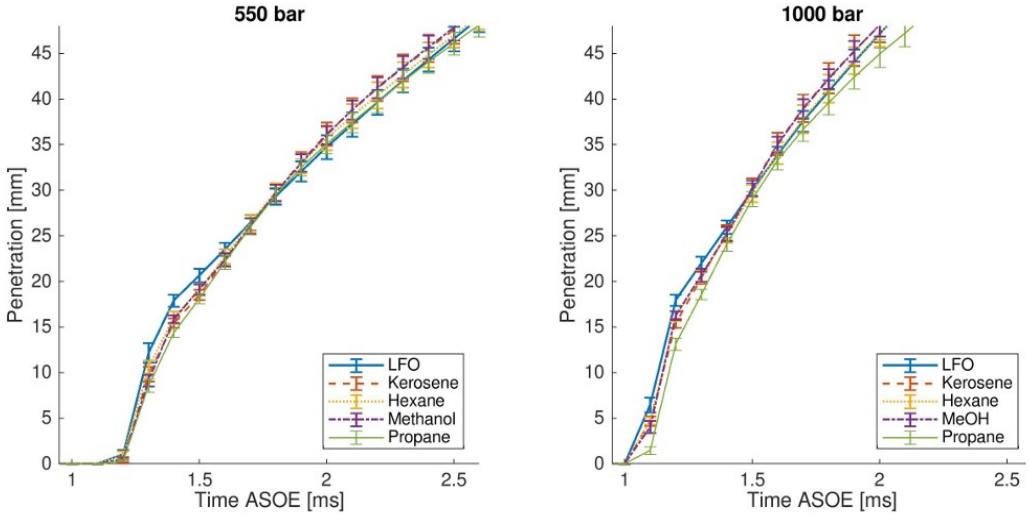

FIG. 11: Spray tip penetration, chamber density 100 kg/m³.

Regarding the effects of increased injection pressure, studies indicate faster penetration (Agarwal et al. 2014, Du et al. 2017, Su and Farrell 1998). A study with a gaseous fuel, liquefied dimethyl ether (DME), indicates slower penetration when compared with diesel fuel (Jun et al. 2001), and the same trend of slower penetration with respect to LFO was also found by Helin et al. (2006) who studied LPG sprays. Furthermore, Yu et al. (2002) conclude that the variations between DME and LFO (diesel fuel) decrease at increased ambient pressures. In general, all these trends are in line with the findings of this study as seen from figures 9 – 11. While DME certainly has different properties than propane, they both are gaseous at room temperatures and seem to have, based on the referred studies, some similarities with respect to LFO.

The shorter penetration of propane sprays can be explained by lower initial momentum due to lower density as well as the loss of momentum during spray evolution as a result of droplet breakup and evaporation. According to Yu et al. (2016), lower viscosity induces smaller droplets in the spray, and this can, together with different densities, explain some of the differences between the fuels. This viewpoint is supported by Dernotte et al. (2012) who conclude that both viscosity and fuel density affect spray penetration and opening angles. While the effect of density was reported to be smaller than that of viscosity, surface tension was found to have no significant effect. However, the penetration curves of kerosene in figure 10 cannot be explained by these parameters and leave room for other studies.

As chamber density is increased, drag forces increase as well, which explains why sprays penetrate slower at increased chamber densities. Furthermore, faster penetration as a result of increased injection pressure can be explained by higher momentum due to increased liquid velocities at the injector nozzle. The higher velocities, resulting from increased injection pressure, can be explained by Bernoulli's well-known equation. Finally, it is noted that despite figure 11 shows almost no differences between propane and the other fuels, figure 7 indicates considerable evaporation at the tip area of the propane spray at the chamber density of 100 kg/m³. While this may seem contradictory at first, the visible evaporation area at the tip region was, nevertheless, dark enough for the analysis script to consider it as “spray area”. It also needs to be noted that the role of spray-to-spray variations cannot be evaluated from figure 7.

3.3 Opening angles

In order to get a better view on the differences in the shapes of the fuel sprays, characteristic opening angles are determined at two different distances (x in fig. 4) from the injector nozzle. In figure 12, the angles have been calculated from the width of sprays at the distance of 20 mm that is approximately 67 times the nozzle orifice diameter. In figure 13, the distance is 40 mm, which describes the width of the spray relatively far from the nozzle. At the closer distance, the response of propane to the increased chamber density is opposite to the other fuels. The differences between the liquid fuels are rather small, albeit kerosene sprays seem to have slightly larger opening angles in most of the test points. Moreover, with 1000 bar injection pressure and 100 kg/m^3 chamber density, LFO sprays seem to have little narrower sprays than kerosene, hexane, or methanol.

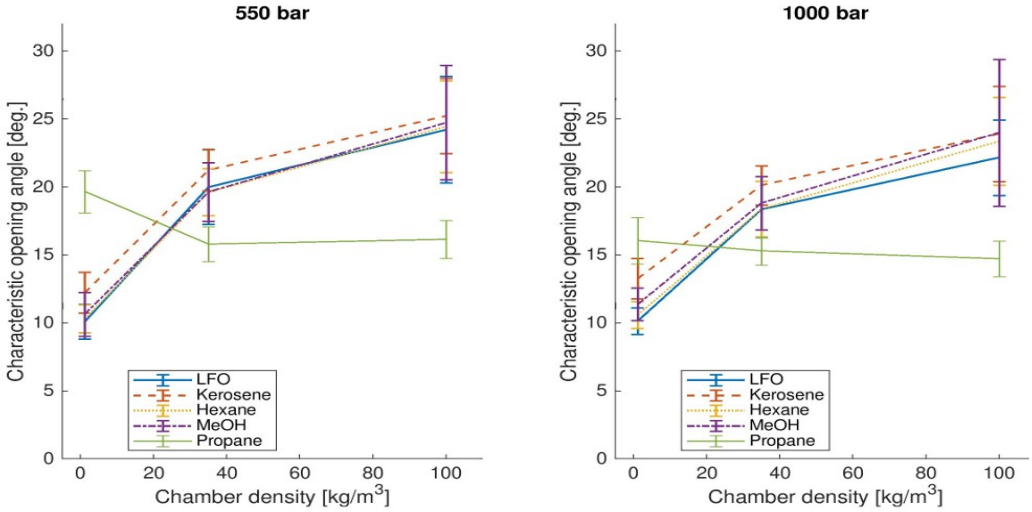

FIG. 12: Effect of chamber density on characteristic opening angles at the distance of 20 mm from the injector. Injection pressures 550 and 1000 bar.

When increasing the observation distance to 40 mm, the different behavior of propane is similarly visible. As chamber density was increased to 100 kg/m^3 and injection pressure to 1000 bar, the mean opening angle of propane sprays decreased to below 5 degrees (fig. 13, right), which indicates, due to the system's inability to detect vapor phase, that the spray was strongly vaporized at the distance of 40 mm from the injector nozzle. Furthermore, the error bar in this point suggests large variations between repetitions and presumably complete vaporization in some repetitions. The differences between the other fuels are again small, and kerosene would seem to be characterized by slightly larger opening angles in most test conditions. Moreover, the angle of LFO sprays seems to have slightly different response to the increase of chamber density. Overall, while it is clear that propane behaves differently due to fast vaporization, the differences between the other fuels in terms of opening angles seem to be rather small. Apart from the cases of 1.2 kg/m^3 chamber density, the standard deviations are also much larger than the differences in mean values between the liquid fuels.

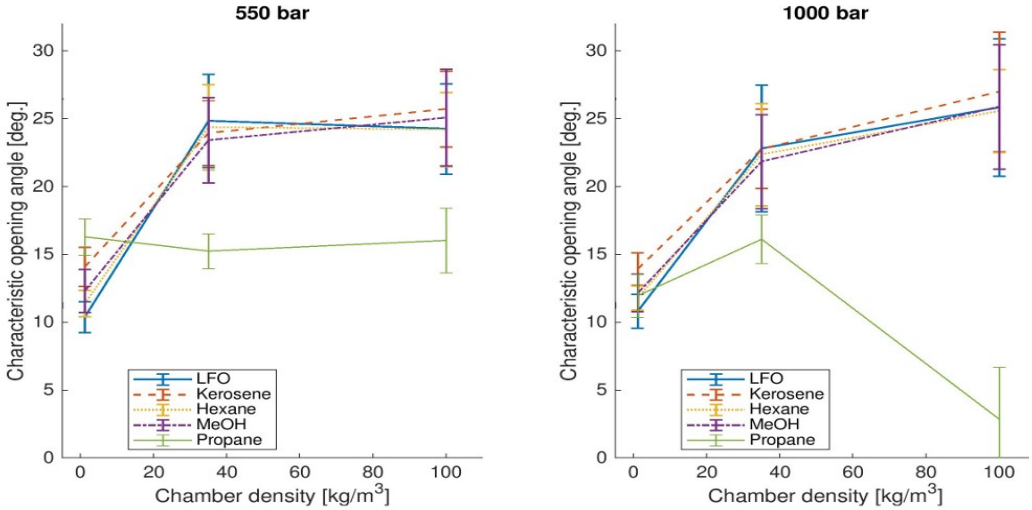

FIG. 13: Effect of chamber density on characteristic opening angles at the distance of 40 mm from the injector. Injection pressures 550 and 1000 bar.

Concerning the effects of injection pressure on spray opening angles, Su and Farrell (1998) have found that an increased injection pressure would decrease opening angles, whereas Mohan et al. (2014) and Wu et al. (2015) present opposite findings. On the other hand, Du et al. (2017) conclude

that injection pressure would not affect liquid phase cone angle, but that an increase in injection pressure would induce wider vapor phase cone angles. In the present study, the effect of increased injection pressure seemed to depend on chamber density, but a slight decreasing effect seems to be more common when combining the results from figures 12 and 13. Thus it can be concluded that the effect of injection pressure on opening angles is not as clear as its effect on tip penetration and injection delay.

The differences in opening angles between propane and the other fuels can be attributed to propane's different properties. Being a light hydrocarbon with only three carbon atoms and having a low boiling point, it vaporizes quickly after being injected into the spray chamber. Combined with an imaging system that can capture only liquid phase fuel, this explains the low measured opening angles of propane sprays at elevated chamber densities. However, propane seems to have wider sprays at the chamber density of 1.2 kg/m³ particularly close to the injector nozzle as seen from fig. 12. This suggests that the liquid propane spray is able to expand transversally, presumably due to stronger turbulence in the injector nozzle, which is a result of propane's low boiling point. As an increased gas-to-liquid density ratio has been reported to increase spray angles (Heywood 1988, Naber and Siebers 1996), it is concluded that the lower density of liquid propane (table 2) have contributed to the observations of wider liquid sprays at the lowest chamber density. Furthermore, this relation between spray angles and gas-to-liquid density ratios also explains why the sprays were, apart from propane, generally wider at increased gas densities.

A study by Helin et al. (2006) indicates that LPG sprays would be characterized by narrower opening angles than diesel fuel sprays, which is in line with the present study except the lowest tested chamber density. Nevertheless, the varying differences of a gaseous fuel with respect to a reference diesel have also been observed by Suh and Lee (2008) who found that the differences between DME and diesel fuel sprays depend on ambient temperature and pressure. Despite the narrower propane spray angles found at elevated chamber densities, the results by Oguma et al. (2003) support the viewpoint that gaseous fuel sprays have large vapor regions around the liquid region.

Among the liquid fuels, kerosene is identified to have slightly larger opening angles in many test points (figures 12 and 13). With respect to LFO, the observation is in line with the results by Yu et al. (2016) who attribute the finding to increased turbulence in the injector nozzle. Increased turbulence, on the other hand, could be a result of decreased viscosity (Dernotte et al. 2012). However, based on kerosene's properties (table 2), it is closer to LFO than any other tested fuel, which suggests that kerosene should differ from LFO less than the other fuels. As this is not the case in the results, the observations could not be fully explained by fuel properties.

3.4 Droplet sizes

As the inner parts of diesel sprays are too dense for shadow imaging techniques, the image area was located at the edge of the spray (fig. 4). The imaging conditions were optically challenging, and despite the selection of images for analysis, image quality left room for improvements. The number of images and detected droplets as well as test variables and calculated mean diameters are collected into table 5. According to Lefebvre (1989), a reasonable accuracy for a droplet size distribution should be achieved with a sample size of 5 000 droplets. While Paine (1993) states that the adequate sample size for acceptable sampling error is not constant, the results of the same reference indicate that a sample of approximately 5000 particles would clearly be on the safe side. In the present study, the number of detected droplets per test point varied roughly between 4 000 and 13 000.

In figure 14, Sauter mean diameters (SMDs) have been plotted against injection pressure and chamber density, suggesting that methanol sprays would contain slightly smaller droplets than LFO sprays. Moreover, it seems that an increase in injection pressure would affect the SMDs of LFO sprays slightly more than those of methanol sprays, and that the differences between the fuels would decrease when increasing both injection pressure and chamber density. The droplet size

distributions (fig. 15) are in line with the calculated SMDs and indicate slight differences between LFO and methanol. However, care should be taken not to highlight the absolute values due to the limitations in image quality and consequently the success of droplet sizing. Instead, the relative differences between LFO and methanol are addressed here.

TABLE 5: Summary of droplet size measurements. D10: arithmetic mean diameter, D32: Sauter mean diameter.

Chamber density [kg/m^3]	Injection pressure [bar]	Fuel	Total number of images	Number of images in the analysis	Share of included images [%]	Number of detected droplets	D10 [µm]	D32 [µm]
35	550	MeOH	149	67	45,0	13388	16,2	23,5
35	1000	MeOH	110	57	51,8	11054	16,0	22,3
100	550	MeOH	270	54	20,0	3707	15,9	23,3
100	1000	MeOH	190	50	26,3	4115	14,5	23,0
35	550	LFO	170	51	30,0	5460	19,3	27,0
35	1000	LFO	180	54	30,0	6689	18,1	25,5
100	550	LFO	270	53	19,6	4364	18,4	26,7
100	1000	LFO	360	56	15,6	4753	15,8	23,8

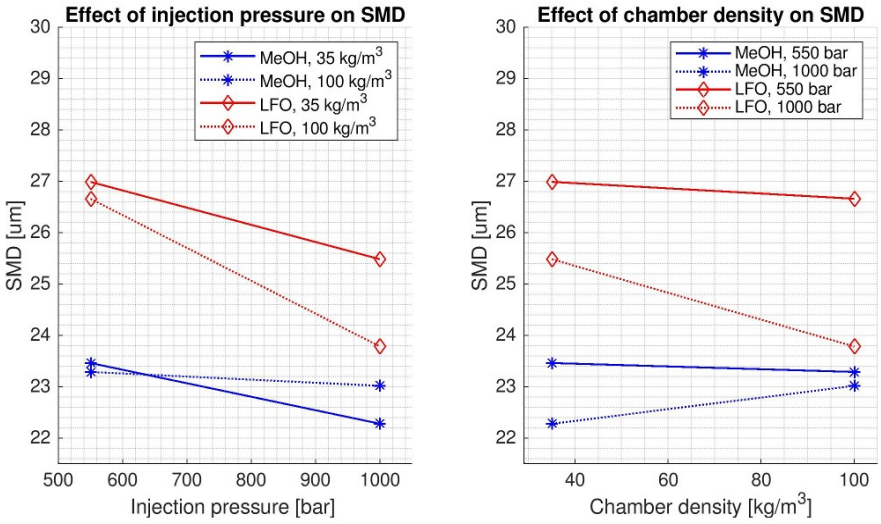

FIG. 14: Effects of injection pressure (left) and chamber density (right) on Sauter mean diameters.

Overall, despite the unavoidable uncertainties related to image quality and automated droplet analysis, the results suggest that methanol sprays would be characterized by slightly smaller droplets than LFO sprays in the measured injection conditions. The trend of smaller droplet sizes with methanol has also been found by Aigal et al. (1986), albeit their results indicated much larger differences. However, the results of the present study do not give support for their findings on methanol's significantly narrower droplet size distributions. It shall also be noted that the results may not be fully comparable due to different test parameters, equipment, and analysis methods.

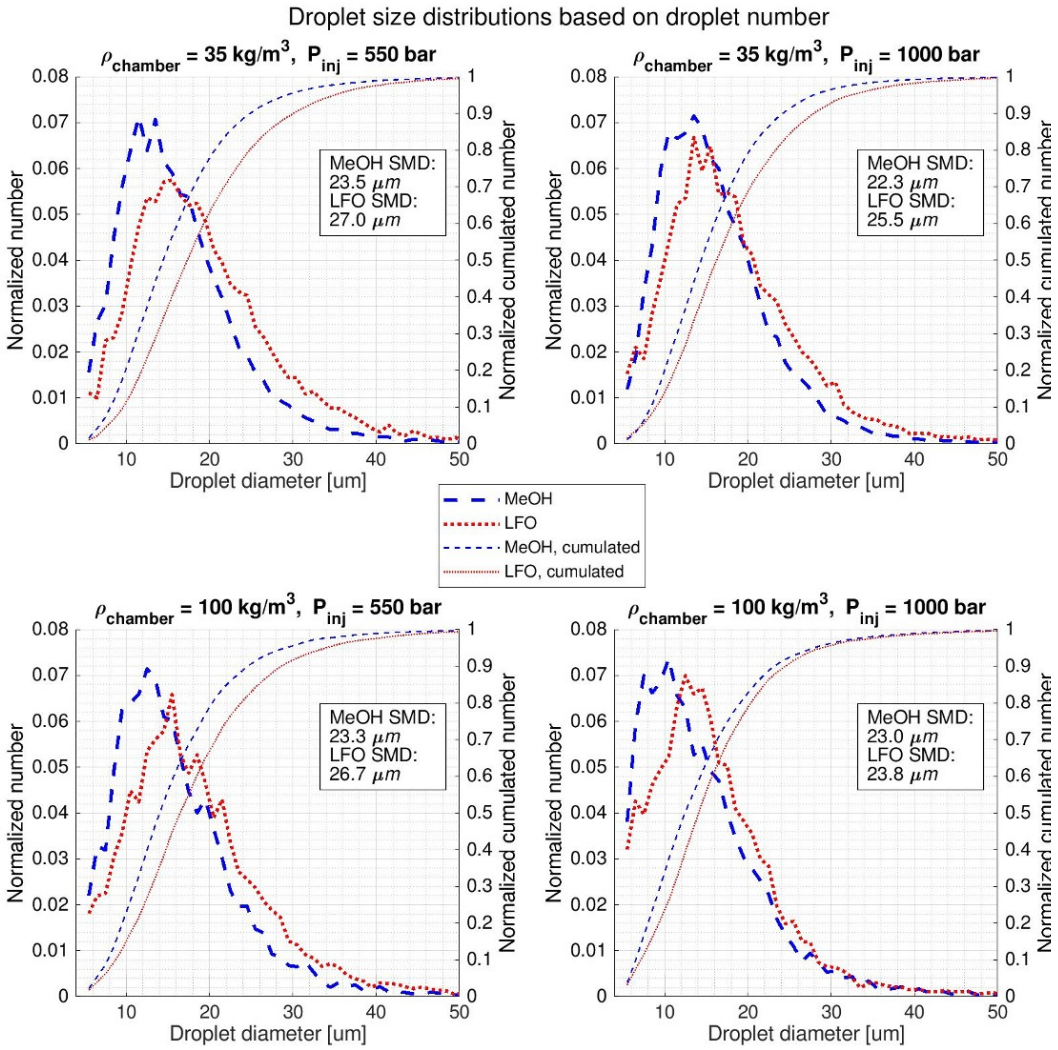

FIG. 15: Droplet size distributions for methanol and LFO.

In spite of the differences in many test parameters (tables 1 and 5), the SMDs of LFO/diesel sprays reported by Hwang et al. (2017) are similar to the SMDs of the present study. Kawaharada et al. (2015) and Komada et al. (2013) have also studied droplet diameters in diesel sprays, and the large range in their reported arithmetic mean diameters covers the results of this study. On the other hand, Cárdenas et al. (2010) have found much smaller diameters, presumably due to substantially higher ambient temperatures.

In literature, an increase in injection pressure is attributed to smaller droplet sizes (Cárdenas et al. 2010, Dernotte et al. 2012, Hwang et al. 2017, Su et al. 1995, Su and Farrell 1998, Wu et al. 2015), and the results of the present study support this viewpoint. On the other hand, the results by Kawaharada et al. (2015) suggest that the effect of injection pressure on droplet sizes would depend on the location of measurements. Regarding the effects of increased fuel viscosity, Dernotte et al. (2012), Goldsworthy et al. (2011), as well as Hiroyasu and Arai (1990) report increased SMDs, and the same trend has been observed with biodiesel and biodiesel blends that are characterized by higher viscosity, density, and surface tension than mineral diesel fuel (Gupta and Agarwal 2016, Hwang et al. 2017). As methanol has lower viscosity, density, and surface tension than LFO, it can be concluded that the findings of this study are in line with the aforementioned studies in terms of the presented fuel properties.

While Dernotte et al. (2012) found that both viscosity and density have an effect on SMDs, they also concluded that viscosity would have a more significant role. Increased viscosity was thought to decrease the amount of turbulence and instabilities in the flow, which results in weaker atomization and hence larger droplet diameters. The small increase in SMDs caused by an increase

in fuel density was suggested to result from the dependance of injection velocity on density when keeping injection pressure constant. Finally, it is generally noted that an increased surface tension should result in larger droplets as this parameter describes the magnitude of cohesive forces in a droplet.

4. CONCLUSIONS

In this study, fuel spray penetration and opening angles were investigated for EN 590 light fuel oil, kerosene, hexane, methanol, and propane. Furthermore, droplet sizes were studied for methanol and light fuel oil sprays from a single location at the edge of the sprays. The fuels were injected from a marine-size common rail diesel injector to a spray chamber filled with pressurized nitrogen, and the results were based on the analysis of shadow images. The main findings of this study can be summarized as follows.

1. Spray penetration: Propane sprays penetrate slower than the sprays of the other fuels, but the differences are decreased and finally almost disappeared when increasing chamber density. From the liquid fuels, apart from the lowest tested chamber density, the tip of LFO sprays seemed to decelerate slightly more after the initial acceleration. Higher injection pressure decreased injection delay, and increased chamber density reduced variations between repetitions.

2. Spray angles: Apart from the chamber density of 1.2 kg/m^3, propane forms significantly narrower sprays than the liquid fuels. This was attributed to propane's fast evaporation that resulted in a narrow liquid spray. With the lowest chamber density, propane sprays were wider especially close to the nozzle. Differences between the liquid fuels were mostly small, but kerosene seemed to form slightly wider opening angles in many test points. With the exception of propane, the fuels had mostly similar responses to increased chamber densities. Variations between repetitions were large in relation to the differences in average values between the liquid fuels.

3. Droplet sizes: The results indicated that methanol sprays would be characterized by slightly smaller droplet sizes than LFO sprays, and that the differences would decrease when increasing both chamber density and injection pressure. The former finding is in line with an earlier study, albeit the found differences were much smaller. Measured mean droplet sizes were decreased with both fuels when increasing injection pressure, but the effect seemed to be slightly stronger with LFO.

Concerning overall spray geometry, subsequent studies could be conducted to reduce the amount of uncertainty regarding the differences between the experimented liquid fuels. For instance, it could not be explained by fuel properties why kerosene had slightly wider sprays in most test points. Furthermore, particularly the knowledge of propane sprays would be largely increased by using a measurement system, such as Schlieren imaging, that is able to detect the vapor phase of sprays. Nevertheless, the obtained results on propane are in line with the main findings of Helin et al. (2006) on propane/butane mixtures. Regarding droplet size measurements, it is acknowledged that high-pressure fuel sprays are a challenging environment for imaging techniques. Together with the limitations in obtained image quality and the shortage of methanol spray droplet sizing studies, the narrow range of applied test parameters, including injection parameters and only one analysis location, leaves room for further studies with various and possibly more advanced measurement techniques. Finally, further research is suggested to study the effects of different injector and nozzle types on droplet sizes while keeping the focus on alternative fuels, such as methanol.

ACKNOWLEDGMENTS

The funding from the European Union HERCULES-2 project within Horizon 2020 research and innovation programme under grant agreement No 634135 is acknowledged. The study has also been financially supported by the Academy of Finland (grant numbers 297248 and 289592). Furthermore, grants were received from Merenkulun säätiö and Henri Fordin säätiö to finalize parts of the presented results.

REFERENCES

Agarwal, A. K., Dhar, A., Gupta, J. G., Kim, W. I., Lee, C. S., and Park, S., Effect of fuel injection pressure and injection timing on spray characteristics and particulate size–number distribution in a biodiesel fuelled common rail direct injection diesel engine, *Applied Enery*, vol. 130, pp. 212-221, DOI: 10.1016/j.apenergy.2014.05.041, 2014.

Aigal, A. K., Pundir, B. P., Khatchian, A. S., High Pressure Injection and Atomization Characteristics of Methanol, SAE Technical Paper 861167, DOI: 10.4271/861167, 1986.

Arai, M., Physics behind Diesel Spray and Its Combustion, Saarbrücken, Germany: Lap Lambert Academic Publishing, ISBN 978-3-659-97160-0, 2016.

Berg, T., Deppe, J., Michaelis, D., Voges, H., and Wissel, S., Comparison of particle size and velocity investigations in sprays carried out by means of different measurement techniques, *ICLASS-2006, 10th International Conference on Liquid Atomization and Spray Systems*, Kyoto, Japan, 2006.

Brusstar, M., Stuhldreher, M., Swain, D., and Pidgeon, W., High Efficiency and Low Emissions from a Port-Injected Engine with Neat Alcohol Fuels, SAE Technical Paper 2002-01-2743, DOI: 10.4271/2002-01-2743, 2002.

Cárdenas, M., Martin, D., and Kneer, R., Experimental Investigation of Droplet Size and Velocity in Clustered Diesel Sprays under High-Pressure and High-Temperature Conditions, SAE Technical Paper 2010-01-2240, DOI: 10.4271/2010-01-2240, 2010.

Choi, K., Lee, D., Roh, H. G., and Lee, C. S., Effect of Injection Parameters on Spray Characteristics of Gas-to-Liquid (GTL), Biodiesel, and Diesel Fuel for a Multi-Hole Injector in a Diesel Engine, *Atomization and Sprays*, vol. 25, no. 12, pp. 1107 – 1125, DOI: 10.1615/AtomizSpr.2015012055, 2015.

Coghe, A. and Cossali, G. E., Quantitative optical techniques for dense sprays investigation: A survey, *Optics and Lasers in Engineering*, vol. 50, no. 1, pp. 46 – 56, DOI: 10.1016/j.optlaseng.2011.07.017, 2012.

Das, M., Sarkar, M., Datta, A., and Santra, A. K., Study on viscosity and surface tension properties of biodiesel-diesel blends and their effects on spray parameters for CI engines, *Fuel*, vol. 220, pp. 769 – 779, DOI: 10.1016/j.fuel.2018.02.021, 2018.

Dave, B. C., Prospects for Methanol Production, In: Wall, J., Harwood, C. S., and Demain, A. L. (eds.), Bioenergy, Washington, District of Columbia, USA: ASM Press, ISBN 978-1-55581-478-6, 2008.

Deng, J., Li, C., Hu, Z., Wu, Z., and Li, L., Spray Characteristics of Biodiesel and Diesel Fuels under High Injection Pressure with a Common Rail System, SAE Technical Paper 2010-01-2268, DOI: 10.4271/2010-01-2268, 2010.

Dernotte, J., Camille, H., Houille, S., Foucher, F., and Mounaim-Rousselle, C., Influence of Fuel Properties on the Diesel Injection Process in Nonvaporizing Conditions, *Atomization and Sprays*, vol. 22, no. 6, pp. 461 – 492, DOI: 10.1615/AtomizSpr.2012004401, 2012.

Desantes, J. M., Payri, R., Salvador, F. J., and Gil, A., Development and validation of a theoretical model for diesel spray penetration, *Fuel*, vol. 85, no. 7, pp. 910 – 917, DOI: 10.1016/j.fuel.2005.10.023, 2006.

Desantes, J., Payri, R., Salvador, F., and Manin, J., Influence on Diesel Injection Characteristics and Behavior Using Biodiesel Fuels, SAE Technical Paper 2009-01-0851, DOI: 10.4271/2009-01-0851, 2009.

Dietsche, K.-H. and Reif, K. (eds.), Automotive Handbook, 8th edition, Plochingen, Germany: Robert Bosch GmbH, ISBN 978-0-7680-4851-3, 2011.

Dolan, G. A., Methanol Production and Utilization, In: Vertés, A. A., Qureshi, N., Blaschek, H. P., and Yukawa, H. (eds.), Biomass to Biofuels: Strategies for Global Industries, Oxford, United Kingdom: Blackwell Publishing, ISBN 978-0-470-51312-5, 2010.

Du, W., Lou, J., Yan, Y., Bao, W., and Liu, F., Effects of injection pressure on diesel sprays in constant injection mass condition, *Applied Thermal Engineering*, vol. 121, pp. 234 – 241, DOI: 10.1016/j.applthermaleng.2017.04.075, 2017.

Esteban, B., Riba, J.-R., Baquero, G., Puig, R., and Rius, A., Characterization of the surface tension of vegetable oils to be used as fuel in diesel engines, *Fuel*, vol. 102, pp. 231 – 238, DOI: 10.1016/j.fuel.2012.07.042, 2012.

Goldsworthy, L., Bong, C., and Brandner, P. A., Measurements of Diesel Spray Dynamics and the Influence of Fuel Viscosity using PIV and Shadowgraphy, *Atomization and Sprays*, vol. 21, no. 2, pp. 167 – 178, DOI: 10.1615/AtomizSpr.2011002336, 2011.

Greenhalgh, D. A. and Jermy, M., Laser Diagnostics for Droplet Measurements for the Study of Fuel Injection and Mixing in Gas Turbines and IC engines, In: Kohse- Höinghaus, K. and Jeffries, J. B. (eds.), Applied Combustion Diagnostics, London, Great Britain: Taylor & Francis, Combustion: An International Series, ISBN 1-56032-938-6, 2002.

Gupta, J. and Agarwal, A., Macroscopic and Microscopic Spray Characteristics of Diesel and Karanja Biodiesel Blends, SAE Technical Paper 2016-01-0869, DOI: 10.4271/2016-01-0869, 2016.

Helin, X., Yusheng, Z., and Huiya, Z., Experimental and Numerical Study on the Characteristics of Liquid Phase LPG and Diesel Fuel Sprays, SAE Technical Paper 2006-32-0076, DOI: 10.4271/2006-32-0076, 2006.

Heywood, J. B., Internal Combustion Engine Fundamentals, International Edition, Singapore: Mc-Graw Hill, ISBN 0-07-100499-8, 1988.

Hillamo, H., Optical Fuel Spray Measurements, Doctoral Dissertation, Aalto University, Department of Energy Technology, ISBN 978-952-60-4378-4, 2011.

Hiroyasu, H. and Arai, M., Structures of Fuel Sprays in Diesel Engines, SAE Technical Paper 900475, DOI: 10.4271/900475, 1990.

Hulkkonen, T., Hillamo, H., Sarjovaara, T., and Larmi, M., Experimental Study of Spray Characteristics Between Hydrotreated Vegetable Oil (HVO) and Crude Oil Based EN 590 Diesel Fuel. SAE Technical Paper 2011-24-0042, DOI: 10.4271/2011-24-0042, 2011.

Hulkkonen, T., Sarjovaara, T., Kaario, O., Hämäläinen, I., and Larmi, M., Experimental Study of Conical Diesel Nozzle Orifice Geometry, *Atomization and Sprays*, vol. 25, no. 6, pp. 519 – 538, DOI: 10.1615/AtomizSpr.2015010383, 2015.

Hwang, J., Bae, C., Patel, C., Agarwal, A. K., and Gupta, T., An Experimental Investigation on Spray Characteristics of Waste Cooking Oil, Jatropha, and Karanja Biodiesels in a Constant Volume Combustion Chamber, SAE Technical Paper 2016-01-2263, DOI: 10.4271/2016-01-2263, 2016.

Hwang, J., Bae, C., Patel, C., Agarwal, A. K., and Gupta, T., Near Nozzle Flow and Atomization Characteristics of Biodiesel Fuels, SAE Technical Paper 2017-01-2327, DOI: 10.4271/2017-01-2327, 2017.

Jasper, J. J., The Surface Tension of Pure Liquid Compounds. *Journal of Physical and Chemical Reference Data*, *v*ol. 1, no. 4, pp. 841 – 1010, DOI: 10.1063/1.3253106, 1972.

Jun, L., Sato, Y., and Noda, A., An Experimental Study on DME Spray Characteristics and Evaporation Processes in a High Pressure Chamber, SAE Technical Paper 2001-01-3635, DOI: 10.4271/2001-01-3635, 2001.

Kaario, O., Vuorinen, V., Hulkkonen, T., Keskinen, K., Nuutinen, M., Larmi, M., and Tanner, F. X., Large Eddy Simulation of High Gas Density Effects in Fuel Sprays, *Atomization and Sprays*, vol. 23, no. 4, pp. 297 – 325, DOI: 10.1615/AtomizSpr.2013006784, 2013.

Kashdan, J., Shrimpton, J., and Whybrew, A., Two-Phase Flow Characterization by Automated Digital Image Analysis. Part 1: Fundamental Principles and Calibration of the Technique, *Particle & Particle Systems Characterization*, vol. 20, no. 6, pp. 387 – 397, DOI: 10.1002/ppsc.200300897, 2003.

Kashdan, J., Shrimpton, J., and Whybrew, A., Two-Phase Flow Characterization by Automated Digital Image Analysis. Part 2: Application of PDIA for Sizing Sprays, *Particle & Particle Systems Characterization*, vol. 21, no. 1, pp. 15 – 23, DOI: 10.1002/ppsc.200400898, 2004.

Kawaharada, N., Sakaguchi, D., Ueki, H., and Ishida, M., Effect of Injection Pressure on Droplet Behavior inside Diesel Fuel Sprays, SAE Technical Paper 2015-01-1841, DOI: 10.4271/2015-01-1841, 2015.

Komada, K., Sakaguchi, D., Tajima, H., Ueki, H., and Ishida, M., Relation between Tip Penetration and Droplet Size of Diesel Spray, SAE Technical Paper 2013-01-1599, DOI: 10.4271/2013-01-1599, 2013.

Lefebvre, A. H., Atomization and Sprays, The USA: Taylor & Francis, Combustion: An International Series, ISBN 0-89116-603-3, 1989.

Li, L., Zhang, X., Wu, Z., Deng, J., and Huang, C., Experimental Study of Biodiesel Spray and Combustion Characteristics, SAE Technical Paper 2006-01-3250, DOI: 10.4271/2006-01-3250, 2006.

Linne, M., Imaging in the optically dense regions of a spray: A review of developing techniques, *Progress in Energy and Combustion Science*, vol. 39, no. 5, pp. 403 – 440, DOI: 10.1016/j.pecs.2013.06.001, 2013.

Mohan, B., Yang, W., Tay, K. L., and Yu, W., Experimental study of spray characteristics of biodiesel derived from waste cooking oil, *Energy Conversion and Management*, vol. 88, pp. 622 – 632, DOI: 10.1016/j.enconman.2014.09.013, 2014.

Naber, J. and Siebers, D., Effects of Gas Density and Vaporization on Penetration and Dispersion of Diesel Sprays, SAE Technical Paper 960034, DOI: 10.4271/960034, 1996.

Nguyen, D-K., Van Craeynest, T., Pillu, T., Coulier, J., Verheist. S., Downsizing Potential of Methanol Fueled DISI Engine with Variable Valve Timing and Boost Control, SAE Technical Paper 2018-01-0918, DOI: 10.4271/2018-01-0918, 2018.

Oguma, M., Goto, S., Sugiyama, K., Kajiwara, M., Mori, M., Konno, M., and Yano, T., Spray Characteristics of LPG Direct Injection Diesel Engine, SAE Technical Paper 2003-01-0764, DOI: 10.4271/2003-01-0764, 2003.

Paine, A. J., Error Estimates in the Sampling From Particle Size Distributions, *Particle & Particle Systems Characterization*, vol. 10, no. 1, pp. 26 – 32, DOI: 10.1002/ppsc.19930100106, 1993.

Shao, J., Yan, Y., Greeves, G., and Smith, S., Quantitative characterization of diesel sprays using digital imaging techniques, *Measurement Science and Technology*, vol. 14, no. 7, pp. 1110 – 1116, DOI: 10.1088/0957-0233/14/7/328, 2003.

Sidu, X., Mingfa, Y., and Junfeng, X., An Experimental Investigation on the Spray Characteristics of Dimethyl Ether(DME), SAE Technical Paper 2001-01-0142, DOI: 10.4271/2001-01-0142, 2001.

Sirignano, W. A., Fluid Dynamics and Transport of Droplets and Sprays, Cambridge, United Kingdom: Cambridge University Press, ISBN 0-521-63036-3, 1999.

Spiekermann, P., Jerzembeck, S., Felsch, C., Vogel, S., Gauding, M., and Peters, N., Experimental Data and Numerical Simulation of Common-Rail Ethanol Sprays at Diesel Engine-like Conditions, *Atomization and Sprays*, vol. 19, no. 4, pp. 357 – 386, DOI: 10.1615/AtomizSpr.v19.i4.40, 2009.

Su, T. F., Chang, C. T., Reitz, R. D., Farrell, P. V., Pierpont, A. D., Tow, T. C., Effects of Injection Pressure and Nozzle Geometry on Spray SMD and D.I. Emissions, SAE Technical Paper 952360, DOI: 10.4271/952360, 1995.

Su, T. F. and Farrell, P. V., Characterization of High-Injection-Pressure Diesel Sprays with Relation to Particulate and NOx Emissions, *Atomization and Sprays*, vol. 8, no. 1, pp. 83 – 107, DOI: 10.1615/AtomizSpr.v8.i1.50, 1998.

Suh, H. K. and Lee, C. S., Experimental and analytical study on the spray characteristics of dimethyl ether (DME) and diesel fuels within a common-rail injection system in a diesel engine, *Fuel*, vol. 87, no. 6, pp. 925 – 932, DOI: 10.1016/j.fuel.2007.05.051, 2008.

Vázquez, G., Alvarez, E., and Navaza, J. M., Surface Tension of Alcohol Water + Water from 20 to 50 °C, *Journal of Chemical & Engineering Data*, vol. 40, no. 3, pp. 611 – 614, DOI: 10.1021/je00019a016, 1995.

Wang, F., Wu, J., and Liu, Z., Surface Tensions of Mixtures of Diesel Oil or Gasoline and Dimethoxymethane, Dimethyl Carbonate, or Ethanol, *Energy & Fuels*, vol. 20, no. 6, pp. 2471 – 2474, DOI: 10.1021/ef060231c, 2006.

Wu, D., Wang, W., Pang, Z., Cao, S., and Yan, J., Experimental Investigation of Spray Characteristics of Diesel-Methanol-Water Emulsion, *Atomization and Sprays*, vol. 25, no. 8, pp. 675 – 694, DOI: 10.1615/AtomizSpr.2015011524, 2015.

Yu, J., Lee, J., and Bae, C., Dimethyl Ether (DME) Spray Characteristics Compared to Diesel in a Common-Rail Fuel Injection System, SAE Technical Paper 2002-01-2898, DOI: 10.4271/2002-01-2898, 2002.

Yu, W., Yang, W., Mohan, B., Tay, K., Zhao, F., Zhang, Y., Chou, S., Kraft, M., Alexander, M. A., Yong, A., and Lou, K., Numerical and Experimental Study on Internal Nozzle Flow and Macroscopic Spray Characteristics of a Kind of Wide Distillation Fuel (WDF) - Kerosene, SAE Technical Paper 2016-01-0839, DOI: 10.4271/2016-01-0839, 2016.

Zhao, H., Laser Diagnostics and Optical Measurement Techniques in Internal Combustion Engines, Warrendale, Pennsylvania, USA: SAE International, ISBN 978-0-7680-5782-9, 2012.